AIAA JOURNAL
Vol. 41, No. 8, August 2003

Influence of Four Kinds of Gradient Magnetic Fields on Hydrogen–Oxygen Flame

Eisuke Yamada,* Masahisa Shinoda,† Hiroshi Yamashita,‡ and Kuniyuki Kitagawa§
Nagoya University, Nagoya 464-8603, Japan

To explore the possibility of flame control by magnetic force, the influence of four kinds of gradient magnetic fields on OH density distribution in a hydrogen–oxygen jet diffusion flame was investigated by numerically solving the equations of reactive gasdynamics and magnetism. Vertically decreasing (case 1), vertically increasing (case 2), horizontally decreasing (case 3), and horizontally increasing (case 4) gradients of magnetic field were considered as model configurations. According to the numerical analysis, because the mass density and the magnetic susceptibility of O_2 gas are much higher than those of other chemical species, the surrounding air containing a lot of O_2 gas is strongly influenced by the magnetic force, and the magnetically induced airflow changes the OH distribution in the flame indirectly. The direction and magnitude of the OH density change significantly depends on the configurations of the gradient magnetic field. Specifically, in cases 1, 3, and 4, the OH distribution migrated to the inside of the flame, but in case 2, it moved toward the outside. However, when the horizontally decreasing gradient of the magnetic field was set up near the burner outlet, as in case 3, the OH density change becomes largest among those in the four cases.

Nomenclature

$\boldsymbol{B}$ = magnetic flux density, T
c_p = specific heat capacity under constant pressure, J/(kg · K)
D_i = mass diffusivity of species i, m^2/s
$\boldsymbol{F}_i$ = magnetic force per unit volume acting on species i, N/m^3
$\boldsymbol{f}_i$ = external body force per unit mass acting on species i, N/kg
$\boldsymbol{g}$ = gravitational force per unit mass, N/kg
g_L = Lande's g factor
h = Planck constant, J · s
h_i = enthalpy of species i, J/kg
k = Boltzmann constant, J/K
m = molecular weight of mixture gas, kg/mol
m_i = molecular weight of species i, kg/mol
N = total number of species i,
N_A = Avogadro number, /mol
p = gas pressure, Pa
R = universal gas constant, J/K · mol
r = radial distance in cylindrical coordinate system, m
S_i = total electron spin momentum of species i
T = absolute temperature, K
t = time, s
u = radial component of mean velocity vector of mixture gas, m/s
$\boldsymbol{V}_i$ = diffusive velocity vector of species i, m/s
v = axial component of mean velocity vector of mixture gas, m/s
$\boldsymbol{v}$ = mean velocity vector of mixture gas, m/s
w_i = production rate of species i, kg/m^3 · s
Y_i = mass fraction of species i
z = axial distance in cylindrical coordinate system, m
θ = azimuthal angle in cylindrical coordinate system, rad
λ = thermal conductivity, J/K · m · s
μ = gas viscosity, Pa · s
μ_B = Bohr magneton, J/T
μ_0 = magnetic permeability of vacuum, H/m
ρ = mass density of mixture gas, kg/m^3
ρ_i = mass density of species i, kg/m^3
χ_i = magnetic susceptibility per unit mass of species i, /kg

Received 8 July 2002; revision received 25 March 2003; accepted for publication 31 March 2003.

*Graduate Student, Department of Energy Engineering and Science, Furo-cho, Chikusa-ku; yamada@ees.nagoya-u.ac.jp.
†Research Student, Department of Aerospace Engineering, Furo-cho, Chikusa-ku; shinoda@micro.nuae.nagoya-u.ac.jp.
‡Professor, Department of Mechanical Engineering, Furo-cho, Chikusa-ku; yamashita@mech.nagoya-u.ac.jp.
§Professor, Research Center for Advanced Energy Conversion, Furo-cho, Chikusa-ku; kuni@apchem.nagoya-u.ac.jp. Member AIAA.

Introduction

SINCE Faraday (1791–1867), it has been well known that combustion flames are affected by magnetic fields. In general, the effects of the magnetic fields on flames can be categorized into two types. One of the magnetic effects is caused by the Lorentz force acting on charged particles in flames, that is, ions and electrons, and it has been studied by a large number of researchers in conjunction with applications to the magnetohydrodynamic power generation, etc. According to Lawton and Weinberg[1] and Weinberg,[2] however, the number densities of ions and electrons is less than 10^{14}/m^3 in a hydrogen flame, even when a small amount of propane is added to enhance the ionization. Compared with the number densities of ions and electrons, the number densities of molecules, radicals, and atoms in the flame are on the order of 10^{24}/m^3. Thus, the amount of ionic species is negligibly small, and the influence of the Lorentz force on ordinary hydrogen flames can be ignored.

There is another magnetic effect due to the magnetic force, that is, the magnetic pressure, acting on nonconductive and paramagnetic chemical species in flames, for example, OH radicals and O_2 molecules, etc. The magnetic force per unit volume acting on species i, $\boldsymbol{F}_i$, is expressed by the following equation[3]:

$$\boldsymbol{F}_i = (1/2\mu_0)\rho Y_i \chi_i \nabla(\boldsymbol{B}^2) \tag{1}$$

that is, the magnetic force is essentially in proportion to the mass density ρY_i and the magnetic susceptibility χ_i of the ith chemical species and the gradient of the square of magnetic flux density $\nabla(\boldsymbol{B}^2)$. In Refs. 4–8, it is reported that this magnetic force changes the shape and the temperature of flames. In Refs. 6–8, the magnetic support techniques of the flames in microgravity environments is discussed. However, the mechanism of such a magnetic effect and its applications to flame control techniques are still under discussion.

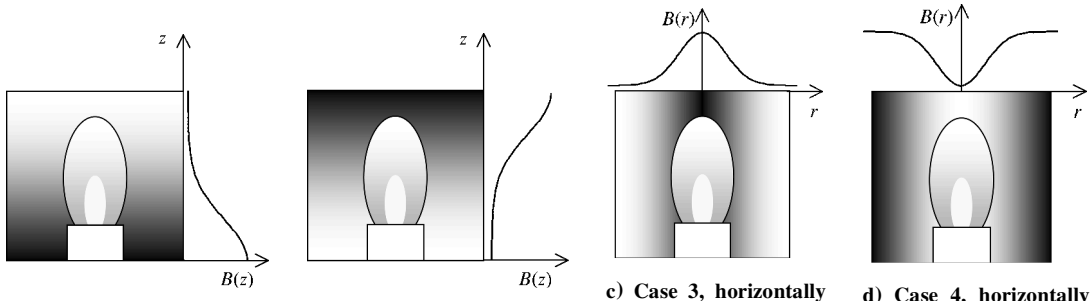

a) Case 1, vertically decreasing gradient magnetic field **b) Case 2, vertically increasing gradient magnetic field** **c) Case 3, horizontally decreasing gradient magnetic field** **d) Case 4, horizontally increasing gradient magnetic field**

Fig. 1 Four kinds of configurations of gradient magnetic field and hydrogen–oxygen jet diffusion flame.

In previous studies,[9–11] it was found from experimental and numerical results that the spatial distribution of OH radicals in a hydrogen–oxygen jet diffusion flame axisymmetrically moved toward the central axis of the flame in the presence of the magnetic field. In particular, according to the numerical analysis,[10,11] the surrounding air containing a lot of paramagnetic O_2 gas was strongly influenced by the magnetic force because the mass density ρY_{O_2} and the magnetic susceptibility of O_2 gas χ_{O_2} are much higher than those of other chemical species. The air was entrained inside the flame at the flame bottom, and this entrainment airflow in the upstream region of the flame changed the OH distribution in the downstream region. That is, the OH distribution migrated passively and indirectly by the convection of mixture gas but not directly by the relative diffusion of OH itself. Consequently, the configuration of the spatial distributions of the O_2 gas and the gradient magnetic field is thought to be a key to controlling the OH density distribution in the flame.

Therefore, in this study, the influence of different spatial distributions of the magnetic field on the OH distribution in a hydrogen–oxygen jet diffusion flame was investigated numerically. Figure 1 shows the four kinds of gradient magnetic fields considered. Here, the origin of the cylindrical coordinate system (r, θ, z) is set at the center of the burner outlet, and the z axis is along the central axis of the flame. In Fig. 1, the monochromatic gradation behind the flame stands for the strength of the magnetic flux density $\boldsymbol{B}(r, z)$. Case 1 is the flame in the vertically decreasing magnetic field (decreasing upward in the z direction), case 2 is in the vertically increasing one (increasing upward in the z direction), case 3 is in the horizontally decreasing one (decreasing outward in the r direction), and finally case 4 is in the horizontally increasing one (increasing outward in the r direction). In practice, the gradient magnetic field generated by magnets has the three-dimensional distribution and both vertical and horizontal components. Therefore, the analysis of these four ideal cases is meaningful in that they give the basis for the practical case. When the results of the four cases are compared with that of the case without the magnetic field, the most effective configuration of the gradient magnetic field is examined for control of the OH distribution in the flame.

Numerical Simulations

The numerical simulations were performed by solving the equations of reactive gasdynamics and magnetism to obtain the OH density distribution in the flame under the external body force.[12,13] The following five equations, that is, the conservation equations of mass, momentum, energy, and chemical species and the state equation, were considered on the (r, z) plane under the assumption of axisymmetry for the cylindrical coordinate system whose origin is set at the center of the burner outlet:

$$\frac{\partial \rho}{\partial t} + \nabla \cdot (\rho \boldsymbol{v}) = 0 \tag{2}$$

$$\frac{\partial (\rho \boldsymbol{v})}{\partial t} + \nabla \cdot (\rho \boldsymbol{v}\boldsymbol{v}) = -\nabla p + \nabla \cdot (\mu \nabla \boldsymbol{v}) + \rho \sum_{i=1}^{N} Y_i \boldsymbol{f}_i \tag{3}$$

$$\frac{\partial (\rho T)}{\partial t} + \nabla \cdot (\rho \boldsymbol{v} T) = \frac{1}{c_p} \nabla \cdot (\lambda \nabla T) - \frac{1}{c_p} \sum_{i=1}^{N} h_i w_i + \frac{1}{c_p} \rho \sum_{i=1}^{N} Y_i \boldsymbol{f}_i \cdot \boldsymbol{V}_i \tag{4}$$

$$\frac{\partial (\rho Y_i)}{\partial t} + \nabla \cdot (\rho \boldsymbol{v} Y_i) = w_i - \nabla \cdot (\rho Y_i \boldsymbol{V}_i) \tag{5}$$

$$p = \rho R T \sum_{i=1}^{N} \frac{Y_i}{m_i} \tag{6}$$

The diffusive velocity of species i, $\boldsymbol{V}_i$, in Eqs. (4) and (5) is given by

$$Y_i \boldsymbol{V}_i = -D_i \left\{ \nabla Y_i - \frac{m_i}{m} \frac{\rho}{p} \sum_{j=1}^{N} Y_i Y_j (\boldsymbol{f}_i - \boldsymbol{f}_j) \right\} \tag{7}$$

For the derivation of Eqs. (2–6), the Soret, Dufour, and pressure diffusion effects, the bulk viscosity, and the viscous dissipation are ignored. The transport coefficients such as D_i, μ and λ are estimated by applying the simplified transport model.[14] The detailed kinetic mechanisms including 9 chemical species (H_2, O_2, H, O, OH, H_2O, HO_2, H_2O_2, and N_2) and 21 elemental reactions[15] are considered for the relevant chemical reactions, and the thermochemical properties of the species are defined from the CHEMKIN database[16] with respect to the temperature and pressure. Furthermore, the direct influence of the magnetic field on the chemical kinetics is ignored by referring to the experimental work by Mizutani et al.[17] They reported that phenomena such as flame propagations, which are dominated by high-speed chemical reactions, are hardly affected by the magnetic field as intense as 5.0 T. Because the magnetic field used in this study is 1.0 T at the highest, we can deal with only the gasdynamic aspect of the magnetic effect, neglecting the chemical kinetic aspect.

The last terms of the momentum and energy equations (3) and (4) indicate the external body force and the mechanical work per unit time by the force, respectively. When Eq. (7) is considered, the last term of the chemical species equation (5) indicates the relative diffusion effect due to the difference of the external body forces acting on chemical species. For instance, the accelerations acting on the species in the gravitational field are the same values for all species, that is, $\boldsymbol{f}_i = \boldsymbol{f}_j$. Then, this term is canceled out. In the gradient magnetic field, however, each species has its own acceleration due to its own magnetic susceptibility, that is, $\boldsymbol{f}_i \neq \boldsymbol{f}_j$. This term appears only in such a special case.

In this study, the external body force per unit mass, $\boldsymbol{f}_i$, acting on species i in Eqs. (3–5) is given by

$$\boldsymbol{f}_i = (1/2\mu_0)\chi_i \nabla(\boldsymbol{B}^2) + \boldsymbol{g} \tag{8}$$

where the Lorentz force on the ionic species is ignored because the density of ionic species is negligibly small in ordinary hydrogen–oxygen flames. The first term on the right-hand side of Eq. (8) is the

magnetic force acting on paramagnetic species only, and the second term is the gravitational force acting on all species. The magnitude of the magnetic susceptibility per unit mass of species i, χ_i, in Eq. (8) mainly depends on the angular momentum of electron spins and orbitals of the substance. When only the former is considered, χ_i is given by Curie's law:

$$\chi_i = \frac{N_A g_L^2 \mu_B^2 S_i(S_i+1)\mu_0}{3kTm_i} \tag{9}$$

which means that the magnetic susceptibility χ_i is essentially in inverse proportion to the absolute temperature T. In Eq. (9), the total electron spin momentum S_i and the molecular weight m_i depend on each chemical species i. The values of S_i for nine typical species in the hydrogen–oxygen flame (H_2, O_2, H, O, OH, H_2O, HO_2, H_2O_2, and N_2) are listed in Table 1. For example, diamagnetic H_2, H_2O, N_2, etc., have no unpaired electron spin, and therefore, there is only slight influence of the magnetic force. On the other hand, paramagnetic O_2, OH, etc., have positive value of χ_i and are affected by the magnetic force because O_2 and OH have two and one unpaired electron spin(s) as shown in Figs. 2a and 2b, respectively. For the spatial distribution of the magnetic flux density $\boldsymbol{B}(r, z)$, the one-dimensional Gaussian function with the standard deviation of 0.010 m is used as the model geometry, and its maximum value is set at 1.0 T. Such a modeling of $\boldsymbol{B}$ is based on the actual measurement of the magnetic flux density produced by an electromagnet. The form of the Gaussian function adopted in each case is as follows.

Case 1:

$$B(z) = 1.0\exp\{-z^2/2(0.010)^2\} \tag{10}$$

Case 2:

$$B(z) = 1.0\exp\left\{-\frac{(z-0.025)^2}{2(0.010)^2}\right\} \tag{11}$$

Table 1 Total electron spin momenta S_i of principal chemical species i in hydrogen–oxygen flame

i	S_i
H_2	0
O_2	1
H	1/2
O	1
OH	1/2
H_2O	0
HO_2	1/2
H_2O_2	0
N_2	0

Case 3:

$$B(r) = 1.0\exp\{-r^2/2(0.010)^2\} \tag{12}$$

Case 4:

$$B(r) = 1.0\exp\left\{-\frac{(r-0.010)^2}{2(0.010)^2}\right\} \tag{13}$$

Figure 3 shows the analytical model used for the numerical simulations. The broken line indicates the calculation domain, ranging from 0 to 12 mm along the r axis and from −5 to 25 mm along the z axis. Thus, the simulations were performed in only one half of the flame by assuming its axisymmetry. Based on the finite volume method, Eqs. (2–5) are constructed in discrete form on the grid mesh of the 61 × 151 points with the mesh width of 0.2 mm. The convection and pressure terms were calculated with the QUICK[18] and SIMPLE[19] methods, respectively. The time integral of Eqs. (2–5) were performed with the implicit scheme of first-order precision using the time interval of 0.2 μs, and the relaxation at each time step was carried out with the successive overrelaxation method. As the boundary conditions, H_2 and O_2 gases, that is, fuel and oxidant gases, were provided from the inner and outer nozzles of the coaxial

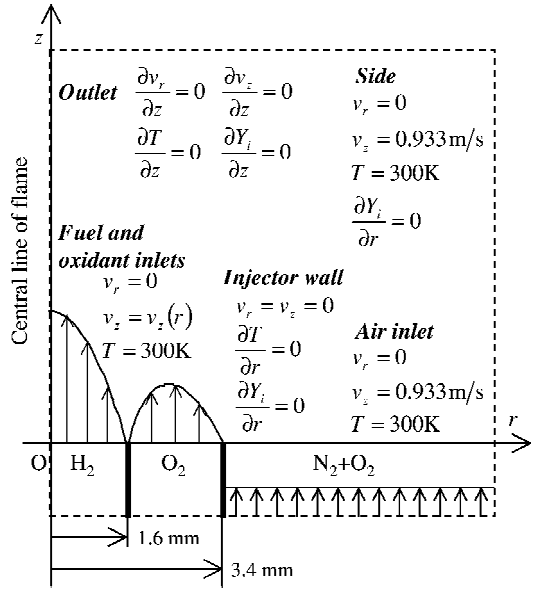

Fig. 3 Analytical model and boundary conditions for numerical simulations.

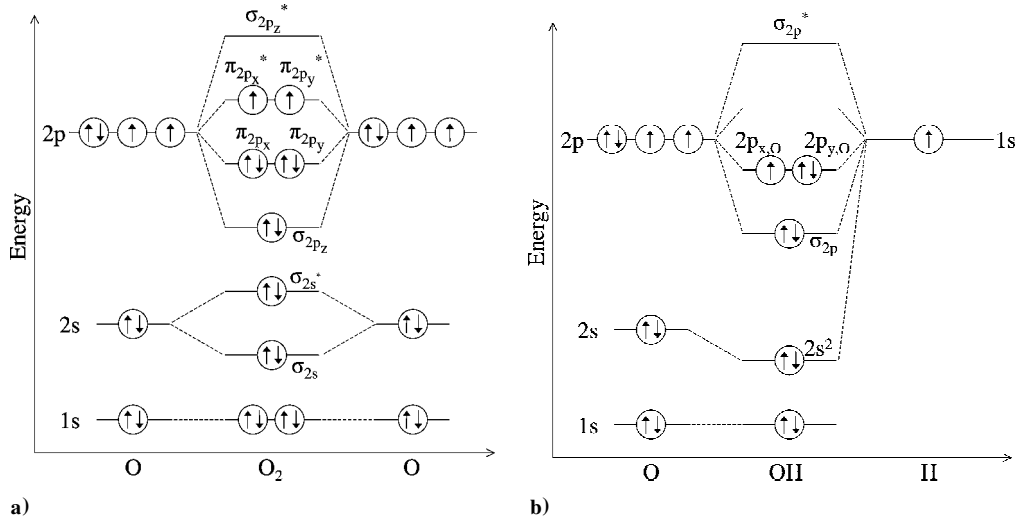

Fig. 2 Electron spins of a) O_2 molecule and b) OH radical.

burner. The velocity profiles of the H_2 and O_2 gases at the burner outlet of $z = 0$ mm were given as Poiseulle flows, that is, the parabolic velocity profile, with the mean flow velocities of 6.79 and 1.06 m/s, respectively, based on previous experimental studies.[9–11] The velocity of the surrounding air (the mixture of 80% N_2 and 20% O_2 gases) at $z = -5$ mm was assumed to be constant at 0.933 m/s. The details of the boundary conditions are also shown in Fig. 3. Except for the spatial distribution of the gradient magnetic field illustrated in Fig. 1, the same conditions were used for cases 1–4.

Results and Discussion

Figures 4a and 4b show the (r, z)-plane two-dimensional distribution of the OH density ρ_{OH} and the mean velocity vectors of the mixture gas, $\boldsymbol{v} = (u, v)$, respectively, in the flame without the magnetic field. The maximum value of ρ_{OH} is over 3000 mg/m^3 in the neighborhood of the burner exit, and the value of $\boldsymbol{v}$ on the central axis of the flame is about 60 m/s at $z = 25$ mm. These results were obtained by numerical simulations under the conditions of steady, two-dimensional (axisymmetric), and laminar flow, and they help in understanding the original flame structure in the absence of the magnetic field.

Figures 5a–5c show the calculated results for the hydrogen–oxygen jet diffusion flame in the vertically decreasing magnetic field (case 1; Fig. 1). First, Fig. 5a shows the magnetically induced change in the (r, z)-plane two-dimensional distribution of the OH density, $\Delta\rho_{OH}$. The change in the OH density distribution was obtained by subtracting the distribution in the absence of the magnetic field from that in presence of the magnetic field. The white area in the monochromatic gradation in Fig. 5a stands for the increase region of the OH density ($\Delta\rho_{OH} > 0$) caused by the magnetic force, whereas the decrease region of the OH density ($\Delta\rho_{OH} < 0$) is shown by the black area. Second, Fig. 5b indicates the magnetically induced change in the (r, z)-plane two-dimensional distribution of the mean velocity vectors of the mixture gas, $\Delta\boldsymbol{v} = (\Delta u, \Delta v)$. Each small arrow in Fig. 5b indicates the relative magnitude and the direction of the velocity vector change that was obtained by subtracting the mean velocity vector in the absence of the magnetic field from that in the presence of the magnetic field. Finally, the five curves in Fig. 5c show the r-direction one-dimensional profiles of the magnetic forces acting on the paramagnetic chemical species with the nonzero magnetic susceptibilities, such as O_2, H, O, OH, and HO_2 listed in Table 1. The magnitudes of these forces acting on species i, F_i, were numerically estimated by Eq. (1) at a height of $z = 10$ mm above the burner outlet. Note that the scale of the magnetic forces shown in Fig. 5c is logarithmic.

In the same way, Figs. 6a–6c show the calculated results for the vertically increasing magnetic field (case 2), Figs. 7a–7c for the horizontally decreasing magnetic field (case 3), and Figs. 8a–8c for the horizontally increasing magnetic field (case 4). In all cases, the gradations of the OH density changes, the arrows of the velocity vector changes, and the curves of the magnetic forces are in the same scale.

At first, we explain the direction and magnitude of the OH density change in each case. As seen in Figs. 5a, 6a, 7a, and 8a, the density variation occurs mainly in the peripheral region of the flame. In Figs. 5a, 7a, and 8a (cases 1, 3, and 4), the increase and decrease regions of the OH density appear inside and outside regions of the flame, respectively. Thus, it is understood that the OH distributions migrate toward the central axis of the flame by the magnetic force. However, in Fig. 6a (case 2), the reverse phenomenon occurs, that is, the increase and decrease regions are seen outside and inside the flame, respectively. Then the OH distribution moves in the outside direction of the flame due to the magnetic effect. When the maximum enhancement and depression values of the OH density change are compared, Fig. 7a (case 3) is more effective than the other three cases, and Fig. 8a (case 4) has the minimum effect. This is more easily understood with Fig. 9, which shows the maximum enhancement and depression values of the OH density change, $(\Delta\rho_{OH})_{max}$, in cases 1–4. When the values in case 3 are compared with those in

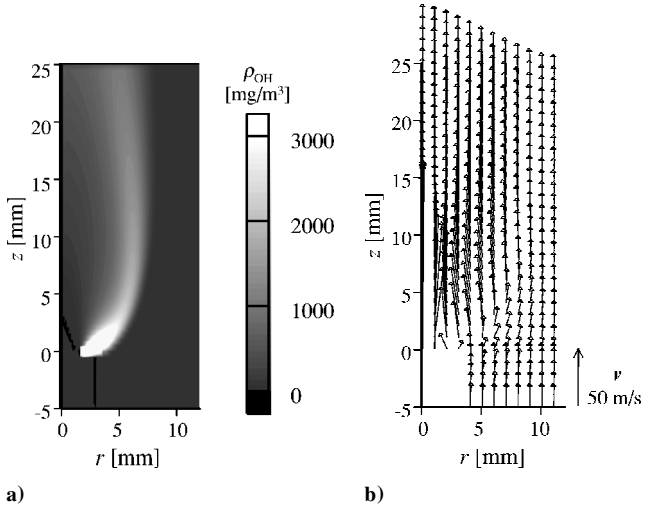

Fig. 4 Distributions in hydrogen–oxygen jet diffusion flame without magnetic field: a) OH density and b) mean flow velocity.

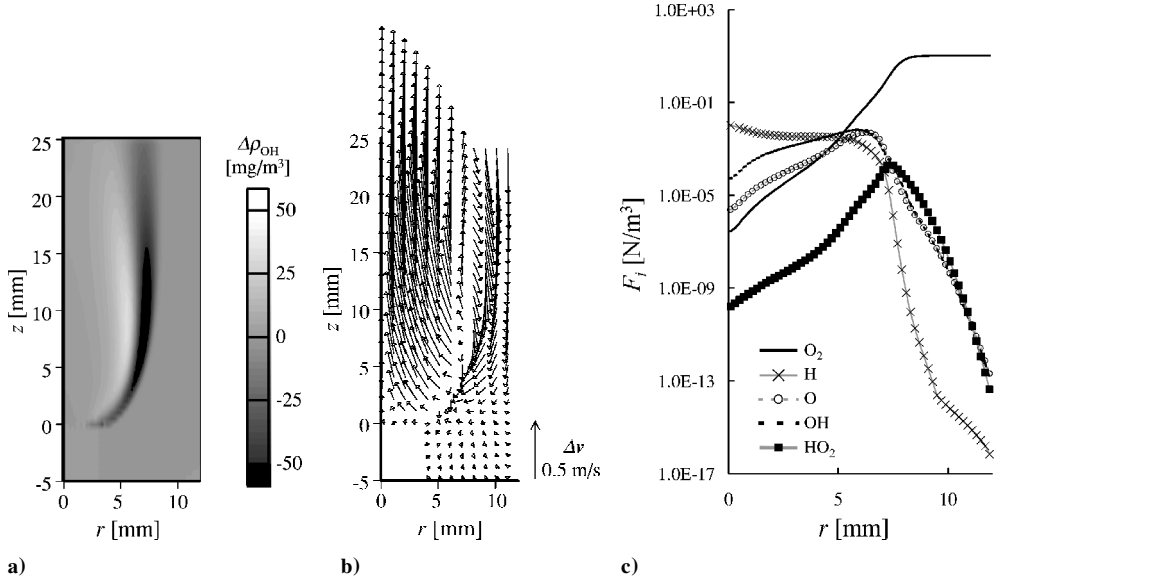

Fig. 5 Case 1: magnetically induced changes in distributions of a) OH density, b) mean flow velocity, and c) magnetic forces acting on paramagnetic species.

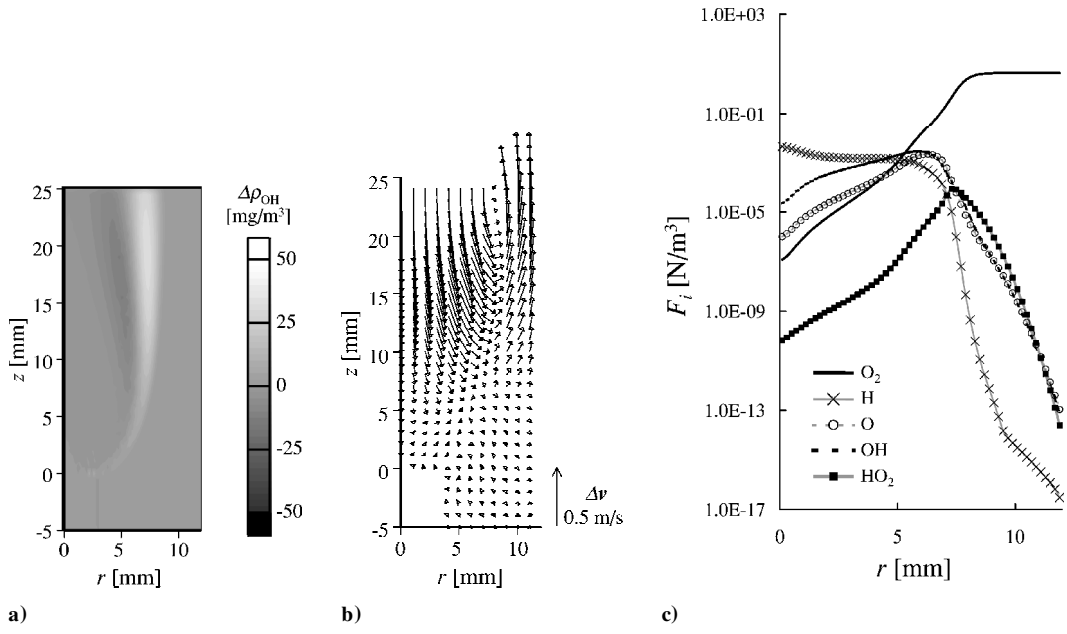

Fig. 6 Case 2: magnetically induced changes in distributions of a) OH density, b) mean flow velocity, and c) magnetic forces acting on paramagnetic species.

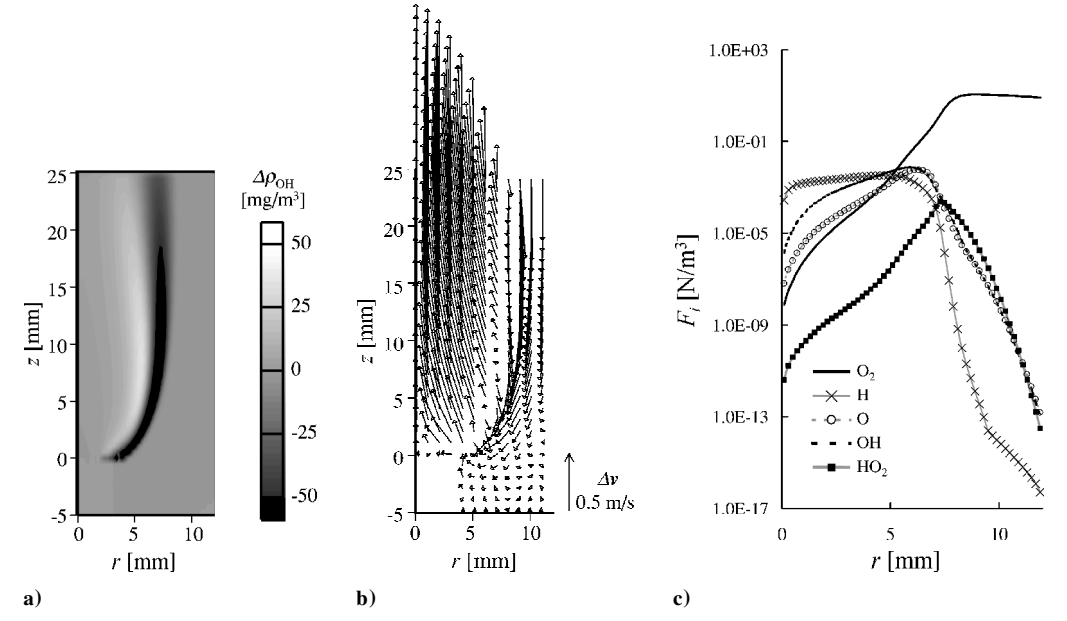

Fig. 7 Case 3: magnetically induced changes in distributions of a) OH density, b) mean flow velocity, and c) magnetic forces acting on paramagnetic species.

case 4, the enhancement value increases from 4 to 34 mg/m^3 and the depression value also increases from -24 to -104 mg/m^3, respectively. That is, the change in the OH density distribution in Fig. 7a (case 3) is about 8.5 times more significant than that in Fig. 8a (case 4) at maximum. In other words, the magnitude of the magnetic effect on the OH density distribution significantly depends on the location of the horizontal gradient of the magnetic field, rather than that of the vertical gradient of the magnetic field. Therefore, by changing the gradient magnetic field along the r axis, the magnetic effect could be drastically varied, or it might become greatest at a certain location. Consequently, it may be possible to control the magnitude of the OH density distribution by adjusting the r-direction gradient of the magnetic field.

Next, we note the flow velocity vectors indicated in Figs. 5b, 6b, 7b, and 8b, and the magnetic forces shown in Figs. 5c, 6c, 7c, and 8c, to examine the physical mechanism of the OH density change in each case. In previous works by the use of experiments and numerical simulations,[9–11] it has been clarified that the OH density change in the flame is caused indirectly by the variation in the mean velocity of mixture gas (the convection of mixture gas), but not directly by the variation in the relative velocity of OH itself (the diffusion of OH itself). In particular, the airflow surrounding the flame is the most important factor. Because the mass densities of paramagnetic chemical species i, ρY_i, in Eq. (1) are very small and the temperature T in Eq. (9) is high in the flame, that is, the magnetic susceptibilities of species i, χ_i, in Eq. (1) are low in the flames, the magnetic forces are negligibly weak at any point in the flames. This is evident from Figs. 5c, 6c, 7c, and 8c. The magnetic forces acting on the paramagnetic species such as O_2, H, O, OH, and HO_2 are less than the order of 10^{-2} N/m^3 inside the flame (in the region of $r < 7$ mm). However, because the mass density and the magnetic susceptibility of O_2 gas, ρY_{O_2} and χ_{O_2}, are much larger than those of the other

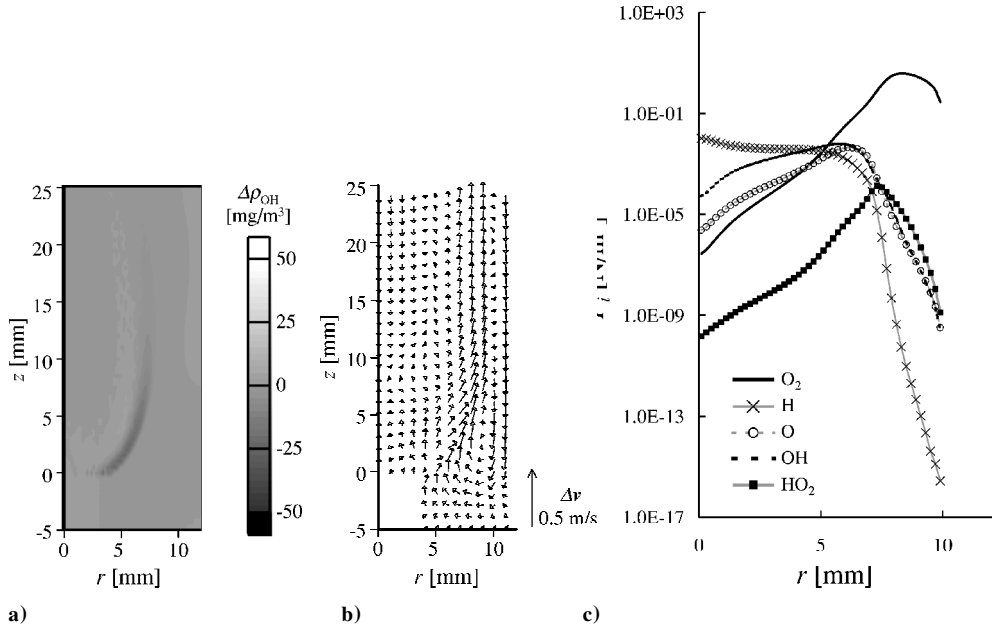

Fig. 8 Case 4: magnetically induced changes in distributions of a) OH density, b) mean flow velocity, and c) magnetic forces acting on paramagnetic species.

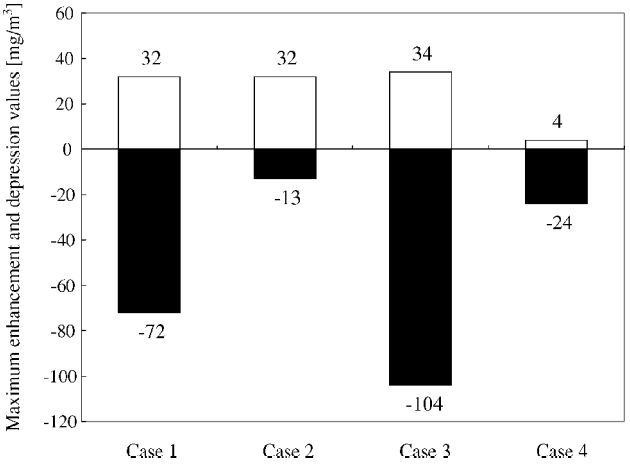

Fig. 9 Maximum enhancement and depression of OH density change.

chemical species in the peripheral region of the flame, only the magnetic force acting on O_2 gas is dominant, and it reaches 10 N/m^3 in the surroundings of the flame (in the region of $r > 7$ mm). That is, the air including a large amount of O_2 gas is strongly affected by the magnetic force in the surroundings of the flame and is accelerated in the direction of larger magnetic flux density. These characteristics are almost the same, and no appreciable differences are found among the profiles of the magnetic forces in Figs. 5c, 6c, 7c, and 8c, except for the slight differences near $r = 0$ mm (the central axis of the flame) in Fig. 7c (case 3) and near $r = 10$ mm in Fig. 8c (case 4). Such minor differences are due to the boundary conditions of the numerical simulations, in that the gradient of magnetic field is zero and the magnetic force also becomes zero at $r = 0$ mm in Fig. 7c (case 3) and at $r = 10$ mm in Fig. 8c (case 4). As a result, it is thought that only the difference in the directions of magnetic forces is the cause of the different results shown in Figs. 5–8 (cases 1–4). Taking account of the directions of the gradient magnetic fields, we can explain the physical mechanism of OH density change in each case.

For example, in Fig. 5 (case 1), which is experimentally the most popular case, the stream of the surrounding air is attracted toward the flame bottom under the vertically decreasing magnetic field (decreasing upward in the z direction). Furthermore, near the flame bottom (in the region of $5 < r < 10$ mm and $0 < z < 5$ mm), the air containing abundant O_2 gas is entrained inside the flame. This behavior of the air can be seen in Fig. 5b. This entrainment airflow causes the change in the OH density distribution in the downstream region of the flame. Thus, the flow of the ambient air at the flame bottom is the key factor involved in the OH density change by the magnetic force.

In Fig. 6 (case 2), the surrounding airflow is induced upward in the presence of the vertically increasing magnetic field (increasing upward in the z direction). Contrarily, the downward stream appears in the inside region of the flame, as indicated in Fig. 6b. Then, the OH density distribution is passively transported in the outside direction by the flow near the flame bottom. However, the change seen in Fig. 6a is smaller than that in Fig. 5a because the maximum gradient of the magnetic field is located at a higher zone above the burner outlet (at $z \sim 15$ mm). If the location of the gradient magnetic field is set nearer the burner outlet, larger changes in the OH density gradation in Fig. 6a and in the flow velocity vectors in Fig. 6b would be obtained.

The result of Fig. 7 (case 3) is similar to that of Fig. 5 (case 1). However, the changes in the OH density in Fig. 7a and in the flow velocity in Fig. 7b are the largest among those of the four cases. In this case, the magnetic force basically acts in the central direction due to the horizontally decreasing magnetic field (decreasing outward in the r direction), and it enhances the entrainment airflow at the location of the maximum gradient of the magnetic field. This enhancement of the entrainment flow at the flame bottom is the reason for the largest changes in the OH density in Fig. 7a and in the flow velocity in Fig. 7b.

Finally, in Fig. 8 (case 4) under the horizontally increasing magnetic field (increasing outward in the r direction), the magnetic force induces the outward direction flow of the surrounding air along the flame edge near the location of $r = 7.5$ mm. However, because this magnetically induced flow cancels out the entrainment flow near the flame bottom, the flow velocity change seen in Fig. 8b is very small. Consequently, the OH density change in Fig. 8a also becomes very small in comparison with those in Figs. 5a, 6a, and 7a.

Thus, by considering the physical mechanism described earlier, we can understand the phenomena seen in Figs. 5–8 (cases 1–4), respectively. As a result, it is recognized that the magnetically induced

flow of the surrounding air including abundant O_2 gas, not that of OH itself, plays a main role in the mechanism of the OH density change in the flame. Because there is a close relationship between the changes in the flow velocity and in OH density, it is important to control the surrounding airflow by adjusting the location of the gradient magnetic field. In particular, when the horizontally decreasing gradient of the magnetic field is set up near the burner outlet, we will be able to obtain the largest change in the OH density distribution, as found in Fig. 7 (case 3). The information obtained in this work may contribute to the development of flame control techniques by the magnetic force.

Conclusions

The following conclusions were obtained by numerically solving the equations of reactive gasdynamics and magnetism to investigate the influence of different spatial distributions of gradient magnetic field on OH density distribution in a hydrogen–oxygen jet diffusion flame. As typical patterns of gradient magnetic field, the vertically decreasing (case 1), the vertically increasing (case 2), the horizontally decreasing (case 3), and the horizontally increasing (case 4) ones were considered.

1) The magnetic force strongly acts on the surrounding air containing abundant paramagnetic O_2 gas. Furthermore, in the region near the flame bottom, the air is entrained inside the flame, and this entrainment airflow causes the OH density change in the downstream region of the flame. That is, the OH density variation is caused indirectly by the convection of mixture gas, but not directly by the relative diffusion of OH itself.

2) The direction of the OH density change is different depending on the different patterns of the gradient magnetic field. In cases 1, 3, and 4, the OH density migrates inside the flame. In case 2, however, the OH density distribution moves outside the flame.

3) The magnitude of the OH density variation sensitively depends on the location of the horizontal gradient of the magnetic field above the burner top, rather than that of the vertical gradient of the magnetic field. In particular, when the horizontally decreasing gradient of the magnetic field is set up near the burner outlet, as in case 3, the OH density change becomes largest among those in the four cases.

Acknowledgment

The authors are deeply grateful to the late Norio Arai, Nagoya University, Japan, for his encouragement.

References

[1]Lawton, J., and Weinberg, F. J., *Electrical Aspects of Combustion*, Clarendon, Oxford, 1969, pp. 214–239.

[2]Weinberg, F. J., *Advanced Combustion Methods*, Academic Press, London, 1986, pp. 331–390.

[3]Abrahams, E., and Keffer, F., *McGraw–Hill Encyclopedia of Science and Technology*, 9th ed., Vol. 10, McGraw–Hill, New York, 2002, pp. 291–293.

[4]Wakayama, N. I., "Effect of a Gradient Magnetic Field on the Combustion Reaction of Methane in Air," *Chemical Physics Letters*, Vol. 188, 1992, pp. 279–281.

[5]Wakayama, N. I., and Sugie, M., "Magnetic Promotion of Combustion in Diffusion Flames," *Physica B: Condensed Matter*, Vol. 216, 1996, pp. 403–405.

[6]Wakayama, N. I., Ito, H., Kuroda, Y., Fujita, O., and Ito, K., "Magnetic Support of Combustion in Diffusion Flames Under Microgravity," *Combustion and Flame*, Vol. 107, 1996, pp. 187–192.

[7]Wakayama, N. I., "Utilization of Magnetic Force in Space Experiments," *Advances in Space Research*, Vol. 24, 1999, pp. 1337–1340.

[8]Fujita, O., Ito, K., Chida, T., Nagai, S., and Takeshita, Y., "Determination of Magnetic Field Effects on a Jet Diffusion Flame in a Microgravity Environment," *Proceedings of the Combustion Institute*, Vol. 27, 1998, pp. 2573–2578.

[9]Yamada, E., Kitagawa, K., Arai, N., Furuhata, T., Hamamura, N., and Zhao, D., "Visualization of Magnetic Effects on Spatial Distributions of OH Radicals in a Hydrogen Flame," *Journal of Flow Visualization and Image Processing*, Vol. 8, 2001, pp. 39–49.

[10]Yamada, E., Shinoda, M., Yamashita, H., Kitagawa, K., and Arai, N., "Magnetic Effects on OH Radical Distributions in a Hydrogen–Oxygen Diffusion Flame," *Proceedings of International Joint Power Generation Conference* [CD-ROM], FACT-19064, American Society of Mechanical Engineers, Fairfield, NJ, 2001.

[11]Yamada, E., Shinoda, M., Yamashita, H., and Kitagawa, K., "Experimental and Numerical Analyses of Magnetic Effect on OH Radical Distributions in a Hydrogen–Oxygen Diffusion Flame," *Combustion and Flame* (submitted for publication).

[12]Williams, F. A., *Combustion Theory*, 2nd ed., Benjamin/Cummings, Tokyo, 1985, pp. 1–18.

[13]Yamashita, H., Djamrak, D., and Takeno, T., "Role of Elementary Reactions in Flame Structure and Unsteady Behavior of Two-Dimensional Fuel Jet Diffusion Flame," *JSME International Journal B*, Vol. 42, 1999, pp. 699–707.

[14]Smooke, M. D., *Reduced Kinetic Mechanisms and Asymptotic Approximations for Methane–Air Flames*, Springer-Verlag, Tokyo, 1991, pp. 1–28.

[15]Gutheil, E., Balakrishnan, G., and Williams, F. A., *Reduced Kinetic Mechanisms for Application in Combustion Systems*, Springer-Verlag, Tokyo, 1993, pp. 177–195.

[16]Kee, R. J., Rupley, F. M., and Miller, J. A., "CHEMKIN-II: A Fortran Chemical Kinetics Package for the Analysis of Gas-Phase Chemical Kinetics," Sandia National Labs., Rept. SAND89-8009, Livermore, CA, Sept. 1989.

[17]Mizutani, Y., Fuchihata, M., and Ohkura, Y., "Pre-Mixed Laminar Flames in a Uniform Magnetic Field," *Combustion and Flame*, Vol. 125, 2001, pp. 1071–1073.

[18]Leonard, B. P., "A Stable and Accurate Convective Modelling Procedure Based on Quadratic Upstream Interpolation," *Computer Methods in Applied Mechanics and Engineering*, Vol. 19, 1979, pp. 59–98.

[19]Patanker, S. V., *Numerical Heat Transfer and Fluid Flow*, McGraw–Hill, New York, 1980, pp. 126–130.

J. P. Gore
Associate Editor